View metadata, citation and similar papers at core.ac.uk
brought to you by CORE
provided by Hochschulschriftenserver - Universität Frankfurt am Main

arXiv:astro-ph/0509325 v2 1 Feb 2006

The outer crust of non-accreting cold neutron stars

Stefan B. Rüster,* Matthias Hempel,† and Jürgen Schaffner-Bielich‡
Institut für Theoretische Physik, J. W. Goethe-Universität,
Max von Laue-Str. 1, D-60438 Frankfurt am Main, Germany
(Dated: November 6, 2006)

The properties of the outer crust of non-accreting cold neutron stars are studied by using modern nuclear data and theoretical mass tables updating in particular the classic work of Baym, Pethick and Sutherland. Experimental data from the atomic mass table from Audi, Wapstra, and Thibault of 2003 is used and a thorough comparison of many modern theoretical nuclear models, relativistic and non-relativistic ones, is performed for the first time. In addition, the influences of pairing and deformation are investigated. State-of-the-art theoretical nuclear mass tables are compared in order to check their differences concerning the neutron dripline, magic neutron numbers, the equation of state, and the sequence of neutron-rich nuclei up to the dripline in the outer crust of non-accreting cold neutron stars.

I. INTRODUCTION

Neutron stars can be observed as pulsars by their light house effect. The matter in non-accreting cold neutron stars is in its ground state in nuclear equilibrium which means that the energy cannot be lowered by strong, weak, or electromagnetic interactions. Matter in equilibrium concerning weak interactions is termed β-equilibrated matter or matter in β-equilibrium. Stars are bound by gravity and have to be charge neutral, otherwise they would be unstable and explode because of repulsive Coulomb forces.

Neutron stars consist of an atmosphere of electrons, nuclei, and atoms. Only a fraction of the electrons are bound to nuclei. The ground state of the nuclei in this regime, with a mass density of $\rho \lesssim 10^4$ g/cm^3, is ^{56}Fe. The equation of state was calculated by Feynman, Metropolis, and Teller [1].

In the context of neutron stars with temperatures above typically 100 eV, a liquid layer is present between the atmosphere and the solid crust due to e.g. hydrogen/helium burning, where nuclei and electrons are in a liquid phase called the "ocean" [2]. However, in this work, we focus on non-accreting neutron stars at zero temperature which is a good approximation for cold neutron stars.

One assumes complete ionization of the atoms, when the spacing between nuclei becomes small compared to the Thomas-Fermi radius $r_{\rm TF} \simeq a_0 Z^{-1/3}$ of an isolated neutral atom. In this equation, a_0 is the Bohr radius and Z the charge number. The mass density approximately amounts to $\rho \simeq A m_u n_N$, where A is the mass number, m_u the atomic mass unit, and n_N the number density of nuclei which depends on the radius of a spheric nucleus whose volume is the average volume per nucleus, $4\pi r_c^3/3 = 1/n_N$ [3]. By combining the last three equations, one finds that the outer crust of cold neutron stars begins when $\rho \sim 10^4$ g/cm$^3 \gg 3AZ$ g/cm^3. This shell consists of nuclei and free electrons. The equation of state was originally calculated by Baym, Pethick, and Sutherland (BPS) [4]. The BPS model is valid for zero temperature ($T = 0$) which is a good approximation for the crust of non-accreting cold neutron stars. We will describe their model of this mass-density regime in more detail in the next paragraph. The inner crust of neutron stars begins when neutrons start to drip out of the nuclei at $\rho \simeq 4.3 \times 10^{11}$ g/cm^3. This happens because the equilibrium nuclei become more and more neutron-rich, and finally no more neutrons can be bound to nuclei. At $\rho \simeq 2 \times 10^{14}$ g/cm^3 nuclei do not exist anymore, signalling the end of the neutron star crust. The equation of state of the inner crust was calculated by Baym, Bethe, and Pethick [5] and another equation of state of this regime was derived by Negele and Vautherin [6]. Also a relativistic mean field model has been used to describe the density regime of the neutron star crust within the Thomas-Fermi approximation (see [7] and references therein). For higher densities, the nuclei disintegrate and their constituents, the protons and neutrons, become superfluid. Muons and hyperons also appear in this shell. The equation of state in this density regime is not well known, but it can be modeled by using non-relativistic many-body theories [8] or relativistic nuclear field theories [9, 10, 11, 12]. At extremely high densities, even the protons, neutrons, and hyperons disintegrate to their constituents, the quarks. If neutron stars with huge central densities exist then they can contain a quark core [13] which probably is color-superconducting [14, 15].

In this paper, we focus on the outer crust of non-accreting cold neutron stars. It contains nuclei and free electrons. The latter become relativistic above $\rho \sim 10^7$ g/cm^3. The nuclei are arranged in a body-centred cubic (bcc) lattice. The contribution of the lattice has a small effect on the equation of state but it changes the equilibrium nucleus to a larger mass number and lowers the total energy of the system because it will minimize the Coulomb interaction energy of the nuclei. The latter are stabilised against β-decay by the filled electron sea.

*Electronic address: ruester@th.physik.uni-frankfurt.de
†Electronic address: hempel@astro.uni-frankfurt.de
‡Electronic address: schaffner@astro.uni-frankfurt.de

At $\rho \sim 10^4$ g/cm^3, ^{56}Fe is the true ground state. With increasing mass density, it is not the true ground state anymore because the nuclei capture electrons, emit neutrinos and become neutron richer. When the mass density $\rho \simeq 4.3 \times 10^{11}$ g/cm^3, the so-called neutron dripline is reached. Neutrons begin to drip out of the nuclei and become free. As soon as neutrons begin to drip out of the nuclei, the outer crust stops and the inner crust begins.

The composition of the outer crust of non-accreting cold neutron stars was investigated by Baym, Pethick, and Sutherland (BPS) in a classic paper 1971 [4]. They calculated the equation of state and the sequence of nuclei which occur in the outer crust of non-accreting cold neutron stars. They used the nuclear data from the droplet model of Myers and Swiatecki [16]. The equation of state of the outer crust of non-accreting cold neutron stars is still commonly taken nowadays from BPS [4] although it is based on nuclear data of the mid sixties of the last century. Haensel, Zdunik, and Dobaczewski (HZD) in 1989 [17] used a Skyrme Hartree-Fock-Bogolyubov (HFB) calculation in spherical approximation for the parameter set SkP [18], hence ignoring effects from deformations, and the droplet model from Myers [19] in order to update the results of BPS. Haensel and Pichon (HP) in 1994 [20] used the experimental nuclear data from the atomic mass table of 1992 from Audi and Wapstra [21] and the theoretical nuclear mass tables of the droplet models from Möller and Nix [22], and Aboussir et al. [23]. A review on the inner and outer crust of accreting as well as non-accreting neutron stars can be found [24].

In view of the previous work, it seems to be more than timely to reinvestigate the properties of the outer neutron star crust with up-to-date and state-of-the-art experimental [25] and theoretical mass tables which became available in the last few years via the Brussels Nuclear Library for Astrophysics Applications (BRUSLIB) [26, 27] and by Dobaczewski and coworkers [28] for Skyrme based models and by Geng, Toki and Meng for a relativistic model [29]. The nuclear models and their mass tables used in this work, as listed in detail in Table I, are taken to update the results of BPS, HZD, and HP. For the first time, the differences of various nuclear models concerning the neutron dripline, magic neutron numbers, the equation of state, and the sequence of nuclei in the outer crust of non-accreting cold neutron stars are investigated in detail. To our knowledge, this work is also the first one which uses mass tables based on modern relativistic nuclear models. Additionally, effects of pairing and deformation of nuclei are studied. We find that the inclusion of deformations for describing nuclei is crucial in determining the composition of the neutron star outer crust.

The results of this work rely on the (unknown) properties of neutron-rich isotopes up to the neutron dripline. The sequence of neutron-rich nuclei found in this work are in reach to be measured by the Facility for Antiproton and Ion Research (FAIR) [30] at the Gesellschaft für Schwerionenforschung (GSI), Darmstadt, by TRIUMF's Isotope Separator and Accelerator (ISAC-II) [31] and by the Rare Isotope Accelerator project (RIA) [32]. Detailed experimental determinations of the binding energy of hitherto unknown nuclei towards the dripline will finally pin down the actual sequence of neutron-rich isotopes in the outer crust of neutron stars. Also, the low density equation of state as well as its composition serves as an important ingredient for low mass neutron star models as well as for neutron star mergers and core-collapse supernovae.

This paper is organised as follows: In Sec. II, we describe how to find the equilibrium nucleus and how to derive the equation of state for the outer crust of a non-accreting cold neutron star by using the BPS model [4]. We use natural units (in units of MeV) and set $\hbar = c = 1$ for the equations presented in the following. We finally convert our results to the cgs-system in order to be able to compare and check the results with BPS. In Sec. III, we describe the nuclear models and their mass tables used in this paper. In Sec. IV, we present our results comparing the various different modern nuclear models and mass tables used here and compare our findings to the previous work of BPS, HZD, and HP [4, 17, 20]. We also show the differences of the theoretical nuclear models concerning the neutron dripline, magic neutron numbers, the equation of state, and the sequence of nuclei in the outer crust of non-accreting cold neutron stars. In Sec. V, we summarize our results.

II. THE BPS MODEL

In order to find the equilibrium nucleus and calculate the equation of state of the outer crust of non-accreting cold neutron stars by using the BPS model [4], one has to treat the pressure P as the independent variable. We start with $P = 9.744 \times 10^{18}$ dynes/cm^2 which corresponds to the mass density $\rho \simeq 1.044 \times 10^4$ g/cm^3. Actually, this special value of the pressure is also the starting value of the pressure in Ref. [4] and the corresponding mass density is in good agreement with the approximation made in Sec. I: $\rho \sim 10^4$ g/cm$^3 \gg 3AZ$ g/cm^3, the mass density at which the outer crust begins. Because the pressure in the star is increasing continuously with decreasing star radius, we increase P until neutron drip is reached, i.e. when the chemical potential of baryons is equal to the neutron mass, $\mu_b = m_n$. With given pressure P, we vary the mass number A, and the charge number Z and solve the equation of the total pressure,

$$P = P_e + \frac{1}{3} W_L n_N \ , \tag{1}$$

for the electronic density n_e. The highest contribution to Eq. (1) is the pressure of free electrons,

$$P_e = \frac{1}{3\pi^2} \int_0^{k_e} \frac{k^4}{E_e} dk \ , \tag{2}$$

where $E_e = (k^2 + m_e^2)^{1/2}$. The electron pressure depends on the electron Fermi momentum which is related to the electron density,

$$n_e = \frac{k_e^3}{3\pi^2} \; . \tag{3}$$

The lattice energy is given by

$$W_L = -1.81962 \, \frac{Z^2 e^2}{4\pi\epsilon_0 a} \; . \tag{4}$$

It has the form of the Coulomb energy with a special prefactor calculated in [33] which arises because of the bcc lattice. The bcc lattice constant a is related to the number density of nuclei by

$$n_N a^3 = 2 \; . \tag{5}$$

The latter one depends on the number density of electrons because of the neutrality condition which has to be fulfilled in stars,

$$n_e = Z n_N \; . \tag{6}$$

The baryon density is related to the number density of nuclei,

$$n_b = A n_N \; . \tag{7}$$

The total energy density is given by

$$E_{\rm tot} = n_N \left(W_N + W_L \right) + E_e \; . \tag{8}$$

The prefactor 1/3 in Eq. (1) originates from the fact that the pressure of the bcc lattice P_L is one third of the energy density of the bcc lattice, $P_L/3 = E_L = W_L n_N$. The energy of the nuclei is obtained by

$$W_N = m_n \left(A - Z \right) + m_p Z - bA \; , \tag{9}$$

where m_n is the neutron and m_p the proton mass, and b is the binding energy per nucleon. The energy density of free electrons amounts to

$$E_e = \mu_e n_e - P_e \; , \tag{10}$$

where

$$\mu_e = \sqrt{k_e^2 + m_e^2} \tag{11}$$

is the chemical potential of the electrons and m_e the electron mass. The quantity to be minimized at fixed pressure P by varying A and Z is the baryon chemical potential

$$\mu = \frac{E_{\rm tot} + P}{n_b} = \frac{W_N + \frac{4}{3} W_L + Z \mu_e}{A} \; . \tag{12}$$

This procedure has been done for different nuclear models. All of them contain data in tabular form for A, Z, or $N = A - Z$, and the corresponding binding energy B or binding energy per nucleon $b = B/A$. We use the data of the nuclear models listed in Table I.

The places at which a phase transition from one to another equilibrium nucleus happens can be found by varying the pressure as long as its difference to the pressure of the precise point of the transition becomes small. As the transition from one nucleus to the next one takes place, P and μ of both phases are equal but there will be jumps in μ_e and n_e when the proton numbers Z of both phases are unequal. The baryon density n_b and the mass density

$$\rho = \frac{E_{\rm tot}}{c^2} \tag{13}$$

will jump accordingly and are approximately given by

$$n_b' - n_b \simeq n_e \left(\frac{A'}{Z'} - \frac{A}{Z} \right) \; , \tag{14a}$$

$$\frac{\Delta\rho}{\rho} \simeq \frac{\Delta n_b}{n_b} \simeq \frac{Z/A}{Z'/A'} - 1 \; . \tag{14b}$$

The adiabatic index Γ is defined by

$$\Gamma = \frac{n_b}{P} \frac{\partial P}{\partial n_b} \; . \tag{15}$$

At the transition point, the adiabatic index jumps to zero because the pressure in both phases is equal.

III. DESCRIPTION OF THE NUCLEAR MODELS USED IN THIS PAPER

In this section, we describe the nuclear models used in this work as listed in Table I. For comparison, we add the results from BPS which were derived by using mass tables from a droplet mass formula from the sixties.

The most recent mass table of the finite range droplet model (FRDM) [34] lists 8979 nuclei ranging from ^{16}O to ^{339}136 extending from the proton dripline to the neutron dripline. The mass table of FRDM is based on a macroscopic finite range droplet model including a folded Yukawa single particle potential. It gives so far the best parameterization of masses of known nuclei throughout the nuclear chart.

Non-relativistic Skyrme parameterizations are the well known and widely used SkM* [35], SkP [36] and SLy4 parameter sets [37]. Set SkM* originates from the parameter set SkM [38] which is fitted to nuclear matter properties and properties of nuclei. Set SkM* is corrected for the systematically too high binding energies and too low fission barriers of set SkM. The set SkP derives from Skyrme-Hartree-Fock-Bogolyubov (Skyrme-HFB) calculations with particular emphasis on pairing effects and the description of neutron-rich nuclei. The parameters are fitted to nuclear matter properties, in particular the symmetry energy and properties of ^{16}O and ^{208}Pb to fix

the surface energy. Also set SLy4 is derived to describe in particular neutron-rich isotopes and the (theoretical) neutron matter equation of state of Wiringa et al. [39] in order to improve the isospin property away from the β-stability line. Nuclear matter properties, the neutron matter equation of state [39], and the binding energies and radii of the doubly magic nuclei ^{40,48}Ca, ^{132}Sn, and ^{208}Pb were utilized for the fit. Mass tables of these parameter sets were performed by Dobaczewski et al. for nuclei up to $Z = 108$ from the proton to the neutron dripline within the Skyrme-HFB approach including effects from deformation and posted at a publicly available web page (see [28]).

The other Skyrme parameterizations are taken from the BRUSLIB web pages [26, 27] and are commonly derived by fitting the masses of about 2000 known nuclei including effects from deformations. Different approximations schemes have been used, however. Sets SkSC4 and SkSC18 use the Extended Thomas-Fermi plus Strutinsky Integral (ETFSI) approximation for the actual calculation of nuclei. The macroscopic part is described by an extended Thomas-Fermi approximation, the shell corrections included by the Strutinsky integral method, and the pairing energy given by the BCS approximation. The binding energy of about 1700 nuclei were fitted to generate mass tables up to $Z = 130, 115$, respectively [26]. The set MSk7 originates from a Skyrme-Hartree-Fock calculation with a ten parameter Skyrme force along with a four parameter δ-function pairing force using the BCS approximation for the pairing energy. Its mass table extends to $Z = 120$ [26]. The sets BSk2, and BSk8, however, are generated by a full Skyrme-HFB calculation. The binding energies of 2149 nuclei were fitted for these latter two sets using the experimental mass table of 2003 [25]. The corresponding mass table contains 9200 nuclei up to $Z = 120$ lying between the neutron and the proton driplines [27]. The newest parameter set along this line, dubbed BSk9, has been constrained by fixing the symmetry energy to 30 MeV [27] and is not considered in the following. All Skyrme based mass tables used in this work take into account effects from deformations. We take the sets SLy4 and BSk8 as state-of-the-art and the most representatives ones for cross comparison to the other approaches used in this work (FRDM and relativistic models).

Relativistic nuclear field theories used here are based on the exchange of mesons or relativistic point-couplings between nucleon fields in the mean-field and the no-sea approximation. The effective Lagrangians behind the parameter sets NL3, NL-Z2, and TMA contain the exchange of scalar, vector, and isovector mesons. Sets NL3 and NL-Z2 include scalar selfinteraction terms, set TMA in addition vector selfinteraction terms in the effective Lagrangian. The parameter set NL3 was developed in particular to describe isospin effects. Besides binding energy and charge radii of 10 nuclei, neutron radii were included into the fit procedure [45]. A selfconsistent microscopic correction to the spurious center-of-mass motion is performed for the set NL-Z2. Its fit encompasses binding energies, diffraction radii, surface thicknesses, charge radii and spin-orbit splittings from a total of 17 nuclei [46]. The recent parameter set TMA [29] updates the sets TM1 and TM2 [48], which were fitted to binding energies and charge radii for low mass numbers (TM2) and high mass numbers (TM1). The fit parameters of the set TMA are chosen to be mass number dependent so as to have a good description of the properties of light and heavy nuclei [29]. Note that the vector field selfinteractions result in a (vector) selfenergy of the nucleon, which is similar to Relativistic Brueckner-Hartree-Fock calculations, therefore mimicking many-body effects of higher order beyond the usual relativistic mean-field description (see e.g. [48] and references therein). The relativistic point coupling model, developed in [47], consists of four, six, and eight-fermion point coupling terms in the effective Lagrangian. Its parameter set PCF1 is determined by a list of similar observables as in the fit for the set NL-Z2 (see above). Pairing effects are usually included by a standard δ-force within the BCS approximation. The mass tables for the sets NL-Z2 and PCF1 range from $Z = 26$ to $Z = 140$, the one for the set NL3 (in spherical approximation) from $Z = 20$ to $Z = 130$ up to several nuclei behind the neutron dripline to look for particle stable neutron-rich islands of stability. Note that only even-even nuclei are computed for our purposes as only those nuclei can possibly appear in the outer crust in nuclear β-equilibrium.

The chiral effective Lagrangian used for the set denoted as 'Chiral' is build on the nonlinear realization of the chiral SU(3)×SU(3) symmetry [40, 41, 42, 43] as motivated from quantum chromodynamics (QCD). The full

Model	Set	Comments	Refs.
Droplet	BPS	used by BPS [4]	[16]
	FRDM	Finite Range Droplet Model	[34]
Experiment		Atomic mass table 2003	[25]
Non-relativistic	BSk2	Skyrme HFB	[27]
	BSk8	Skyrme HFB	[27]
	MSk7	Skyrme HF + BCS	[26]
	SkM*	Skyrme HFB	[28, 35]
	SkP	Skyrme HFB	[28, 36]
	SkSC4	ETFSI method + BCS	[26]
	SkSC18	ETFSI method + BCS	[26]
	SLy4	Skyrme HFB	[28, 37]
	SLy4HO	Skyrme HFB	[28, 37]
Relativistic	Chiral	Chiral effective model	[40]-[43]
	NL3	Nuclear field theory	[44, 45]
	NL-Z2	Nuclear field theory	[46]
	PCF1	Point coupling model	[47]
	TMA	Nuclear field theory	[29]

TABLE I: The nuclear models used in this paper.

nonet of scalar, pseudoscalar, vector mesons is taken into account as well as the baryon octet in the mean-field and no-sea approximation and a dilaton field. The hadron masses, meson masses and baryon masses, are not additional input parameters but are generated by the vacuum expectation values of the scalar fields of the effective Lagrangian (spontaneous chiral symmetry breaking besides explicit symmetry breaking) as dictated by the properties of QCD. Pairing effects are included by the BCS scheme. The SU(3) chiral model describes nuclear matter as well as properties of nuclei [40, 42], hypernuclei [41] and neutron stars [11, 12, 43]. The mass table used extends from $Z = 16$ to $Z = 100$.

For the relativistic models, spherical calculations with and without pairing effects have been performed for the sets NL3, NL-Z2, PCF1 and Chiral. Mass tables of calculations including effects from deformations are publicly available for NL3 [44] and TMA [29] and are taken for comparison to FRDM and the Skyrme-based parameterizations. The mass table for NL3 of [44] lists 1315 even-even nuclei up to $Z = 98$ using the BCS pairing scheme with constant pairing gaps, while the one for TMA [29] contains nuclei from the neutron to the proton dripline up to $Z = 100$ with BCS type δ-force pairing.

IV. RESULTS

In this section, we present our results obtained within the model of Baym, Pethick, and Sutherland (BPS) [4] as the equation of state and the sequences of nuclei of the outer crust of non-accreting cold neutron stars. Various nuclear models as listed in Table I are used for this purpose. As shown in Sec. II, the binding energy B or rather the binding energy per nucleon b together with the mass number A and the proton number Z are the input parameters for the BPS model, see Eq. (9). Different nuclear models, of course, usually have different binding energies per nucleon for the same nuclei resulting in different sequences of neutron-rich nuclei in the outer crust of non-accreting cold neutron stars. Because most of the binding energies of nuclei with low mass numbers are known precisely from experiments, we prefer using the nuclear data from the atomic mass table 2003 from Audi, Wapstra, and Thibault [25] whenever possible. In this context, we mention that we do not take any estimated (non-experimental) data of the atomic mass table [25] into account. If the corresponding nuclei are not listed in the atomic mass table [25], we use the data of theoretical nuclear models for calculating the sequences of nuclei which are present in the crust of non-accreting cold neutron stars. There is only one exceptional case: The nuclear data of the droplet model from Myers and Swiatecki [16] which is used for calculating the original sequence of nuclei obtained by BPS is not modified by nuclear data from the atomic mass table [25] because we want to compare our new results with the original ones from BPS [4]. By using the newest and most modern nuclear models, we update the results of [4, 17, 20].

Besides, we study differences between the theoretical nuclear models directly. The location of the neutron dripline is of great importance for our investigations, because their position in the nuclide chart is decisive if a neutron rich nucleus has a chance to be present in the outer crust of a non-accreting cold neutron star or not. If the nucleus is behind the neutron dripline, it is unstable and will emit neutrons even for β-equilibrium and large electron fractions. Therefore, the nucleus can not be present in the sequence of nuclei in the outer crust. Of course, this is not the case if the nucleus is located before the neutron dripline.

In this section, we subdivide our results in several categories in order to have a better structure of the results in our paper. In Sec. IV A, we show the equations of state by using various nuclear models. In Sec. IV B, we discuss the effect of pairing on the neutron dripline and on the sequence of nuclei. In Sec. IV C, the non-relativistic parameterizations of BRUSLIB [26, 27] and Dobaczewski [28] are compared. In Secs. IV D and IV E, we compare relativistic and non-relativistic models for the neutron dripline and sequences of nuclei to each other. In Sec. IV F, we show the results for the state-of-the-art nuclear models and discuss their proton numbers in the sequences of nuclei. Finally, in Sec. IV G, we make a comparison to previous works.

A. Equations of State

Fig. 1 shows the equations of state, i.e. the pressure as a function of the mass density. For low mass densities, the nuclei appearing in the outer crust of non-accreting cold neutron stars are the same for all nuclear models because they are given by the experimental data of the atomic mass table [25]. Hence, the equations of state in Fig. 1 are almost the same. Only the set BPS exhibits a different sequence of nuclei, because ^{66}Ni is not found as an equilibrium nucleus by using the data from the droplet model from Myers and Swiatecki [16]. But as one can see, this little deviation in the sequence of nuclei does not have any noticeable consequences on the equation of state by comparing to all other graphs. A closer look reveals tiny jumps in the mass density for constant pressure. This is not surprising because such a behaviour is predicted by BPS [4] and explained in Sec. II, see Eqs. (14). Only small differences can be seen in the high density range where the graphs begin to separate. In order to really see these tiny differences, we zoomed into the high mass density region. The jumps and the separation of the graphs are clearly recognizable in Fig. 2. At high mass density, the graphs separate from each other because we use different nuclear models which have different binding energies per nucleon for the same nuclei. This leads to different equilibrium nuclei and different equations of state. The equilibrium nuclei of known nuclei are marked along the graph. The iron nucleus ^{56}Fe

is the energetically favoured one until the energy density reaches 10^7 g/cm^3. Then the sequence of nuclei continues with the nickel isotopes ^{62}Ni, ^{64}Ni, and ^{66}Ni and jumps then to the heavier nuclei ^{86}Kr and ^{84}Se. Beyond ^{84}Se and a energy density of about 10^{10} g/cm^3, we find that the sequence depends on the nuclear model and the nuclear mass table used.

In Fig. 3, we show the adiabatic index Γ as a function of the mass density. As one can see, there are no noticeable differences between the graphs of the nuclear models used. At high mass density, Γ asymptotically approaches the value of the relativistic limit, i.e. $\Gamma = \frac{4}{3}$. At the transition points from one equilibrium nucleus to another, the value of the adiabatic index jumps to zero. For simplicity, these jumps are not shown in Fig. 3.

B. Spherical Relativistic Models and Effects of Pairing

In Fig. 4, the effect of pairing in nuclei on the neutron dripline and on the sequence of nuclei in the outer crust of non-accreting cold neutron stars is depicted. We compare relativistic nuclear models with pairing to those without pairing effects for spherical calculations. The form of the neutron dripline shows some distinct features (but note for the following discussion that the mass tables for NL-Z2 and PCF1 start only at $Z = 26$). In particular, there are 'plateaus' and 'walls' visible along the neutron dripline indicating particular strong shell effects for neutrons as well as protons. In addition, the neutron dripline does not continuously increase with increasing neutron number, but exhibits 'peninsulas' of particle stable isotopes, especially pronounced for the set NL-Z2 (with pairing) around $N = 90-100$ and $Z = 32$. Hence, a sequence of stable isotopes with increasing neutron number stops first at the neutron dripline followed by a region of unstable isotopes, but then exists again a sequence of stable isotopes for higher N. These features were only found because the calculations did not stop at the neutron dripline but were performed even for several nuclei behind the neutron dripline. We also note, that the effect of pairing on the neutron dripline is rather small. The inclusion of pairing does not shift the neutron dripline but smoothes out the neutron-dripline.

The effect of pairing on the sequence of nuclei is also rather small. Differences in the equilibrium nuclei can be only seen at large mass numbers A. For low mass numbers, there is no difference because we use consistently the data of the atomic mass table [25] whenever available. However, pairing has an effect on the sequence of neutron numbers as it splits those of the point coupling model PCF1 and the chiral model: from 82 to 80 and 82 in the point coupling model PCF1 and from 70 to 68 and 70 in the chiral model. The reason is that the effect of pairing leads to the occupation of extra energy levels which are preferred in comparison to the ones without pairing. The smearing of energy levels also cause the smoothing effect on the neutron dripline. Note, that the chiral model does not have the usual magic neutron number 82 but the magic neutron number 70. This effect might be related to the inclusion of tensor terms in the chiral model which are absent in the other relativistic models used here.

C. Non-relativistic Parameterizations

In Figs. 5 and 6, we compare non-relativistic Skyrme-type models. There are no big differences visible for the neutron dripline and the sequence of nuclei between the parameter sets SkSC4, which uses the ETFSI method, MSk7, a Hartree-Fock calculation with BCS pairing, and BSk8, the full HFB calculation, in Fig. 5. The neutron driplines of all models in Fig. 5 are next to each other and the sequence of nuclei are almost the same. Only the set BSk8 has a shift to larger proton numbers Z in the sequence of nuclei, $\Delta Z = 2$. All parameterizations shown in Fig. 5 have magic neutron numbers 50 and 82. On the other hand, the nuclear models of Dobaczewski et al. show pronounced differences in the neutron dripline as well as in the sequences of nuclei, see Fig. 6. The neutron dripline of the set SkP is shifted to smaller proton numbers compared to the set SLy4. The neutron dripline of the set SkM* is shifted to even smaller proton numbers in comparison to the neutron dripline of the set SkP. The sequence of nuclei of the set SLy4 is shifted to larger proton numbers in comparison to the other two sets, with $\Delta Z_{\max} = 4$. The sequence of nuclei for SkP makes an unusual big jump to the nucleus ^{86}Fe and has also unusual magic proton numbers 30 and 38 while the other two sets only have the magic proton number 28. However, all models in Fig. 6 have magic neutron numbers 50 and 82. We conclude, that the details of the approximation, ETFSI, BCS, or HFB, are not important for the location of dripline and the sequence of neutron-rich nuclei in neutron star matter, as long as the parameters are fitted to a similar (extended) set of observables. There are, however, substantial differences if different sets of observables are used for the fitting procedure. Note, that all mass tables used here include effects from deformations.

D. Neutron Driplines

We now compare relativistic and non-relativistic parameter sets and mass tables in detail, delineating in particular the role of deformations. In Fig. 7, we show the neutron driplines of all parameter sets as listed in Table I including the relativistic parameterizations NL3 and TMA within a calculation including deformations.

By comparing the relativistic models with and without pairing, one again recognizes that pairing makes the neutron driplines smoother. The prominent proton number found in the dripline of the point coupling model PCF1 with pairing is 40. Its neutron numbers are 68,

80, and 110 with pairing, and 70, 82, and 112 without pairing. The corresponding proton numbers of the chiral model are 24, 42, and 46 with pairing, and 24, 38, 42, and 46 without pairing. Its neutron numbers are 60, 68, and 110 with pairing, and 62, 70 and 112 without pairing. The proton number found for the model NL-Z2 with and without pairing is 32. Its neutron numbers are 68, 82, 102, and 112 with pairing, and 70, 82, 102, and 112 without pairing. NL3 with pairing has many distinctive steps in the dripline, the proton numbers are 26, 32, 38 and 40. The neutron numbers also for NL3 without pairing are 62, 70, 82 and 112. By comparing spherical with deformed nuclei, one finds that the effect of deformation is that the neutron dripline rises steeper and nearly linear. The neutron driplines of the relativistic nuclear models with deformations, NL3 and TMA, extend from $(Z, N) \simeq (20, 45)$ to $(Z, N) \simeq (50, 105)$ in a nearly linear and direct way in stark contrast to the wiggly neutron driplines of the spherical relativistic calculations. The set TMA has less pronounced neutron and proton numbers in the neutron dripline in comparison to the spherical calculations. Noticeable occupied proton numbers of the model TMA are 22, 26, and 40 which is unusual, and a magic neutron number is 82. In some cases, the neutron dripline steps down before continuing upwards for the mass table of set TMA (at $Z = 30$, $N = 74$ and at $Z = 38$, $N = 88$). The model NL3 with deformations has the proton numbers 30 and 44, the neutron numbers are 54, 82 and 86. Compared to the spherical calculations, the deformed calculations of NL3 and TMA show a rather similar straight behaviour, although the precise endpoint of a certain sequence of isotopes can differ drastically, in particular for $Z = 28$. It is evident, that the inclusion of deformations is crucial for the overall shape of the neutron dripline but that the location depends strongly on the parameterization.

We now discuss the (deformed) Skyrme calculations in comparison. All neutron driplines of the nuclear models taken from BRUSLIB do not show big differences. Only the neutron dripline of the model SkSC18 decreases sometimes to much lower proton numbers Z and then quickly rises again. We attribute this effect to the approximate treatment of shell corrections to the binding energy which will be particular important close to the dripline. All neutron driplines extracted from the BRUSLIB mass tables range from $(Z, N) \simeq (20, 48)$ to $(Z, N) \simeq (50, 108)$ in a nearly linear fashion. A noticeable proton number in the models of BRUSLIB is 30 and the neutron number 82. By comparing the nuclear models from BRUSLIB with the ones from Dobaczewski et al., one can see that there are no substantial differences between the location of the neutron driplines. Only the neutron driplines of the models SkM* and SkP are shifted to lower proton numbers compared to the other parameter sets. The neutron driplines of the sets SLy4 and SLy4HO (set SLy4 calculated in hydrogen oscillator basis) extends from $(Z, N) \simeq (20, 48)$ to $(Z, N) \simeq (50, 108)$ while that one of the set SkM* goes from $(Z, N) = (20, 56)$ to $(Z, N) = (46, 115)$, and the one from the model SkP from $(Z, N) = (20, 46)$ to $(Z, N) = (50, 114)$. By comparing the neutron driplines of the models from Dobaczewski et al. to those from BRUSLIB, one recognizes that there are much more marked shells effects in the models from Dobaczewski et al. Noticeable proton numbers of the models SLy4 and SLy4HO are 32, 42, and 46 and the neutron number 82. A marked proton shell of the set SkM* is 30. A marked neutron shell of this set is 82. The set SkP exhibits the unusually proton number 22 in its dripline, like the relativistic set TMA. The set SkM* exhibits a noticeable downward sequence of the neutron dripline around $Z = 40$ and $N = 100$. Similar features of downward shifts in the neutron dripline are seen in the sequences of the parameter sets from BRUSLIB around $N = 104$ and $N = 108$. We checked that these features are also present for the HFB set BSk8 and not due to the approximation scheme used (BCS or ETFSI).

The neutron dripline of the finite range droplet model FRDM ranges from $(Z, N) = (20, 50)$ to $(Z, N) = (50, 112)$. It has four pronounced proton numbers: 28, 34, 44 and 48. A noticeable neutron shell is again 82. By comparing all neutron driplines from Fig. 7, one recognizes that all non-relativistic models show the magic neutron number 82 to be present at the neutron dripline and that all proton shell closures of the non-relativistic models are less noticeable in comparison to it. These findings are different to the ones for the relativistic models (even when including deformations) in Fig. 7 where both, proton and neutron shells, are more noticeable.

E. Sequences of Nuclei

In Fig. 8, we show the sequences of nuclei in the outer crust of non-accreting cold neutron stars by using various nuclear mass tables. By comparing the sequences of nuclei with pairing to those without pairing, one recognizes that pairing has the effect of splitting the magic neutron numbers. The magic neutron number 82 is split into 80 and 82 in the chiral model and in the point coupling model PCF1. By comparing spherical with deformed calculations, one can see that the effects of deformation on the sequence of nuclei is small. Models with and without deformation have the same magic neutron numbers: 50 and 82. They also have the same sequence of neutron-rich nuclei in the nuclear chart. An exceptional case is the sequence of nuclei of the chiral model which shows differences concerning the magic neutron numbers. The sequence of nuclei within the chiral model does not follow the magic neutron number 82 but instead continues down the neutron number 70 basically all the way to the neutron dripline. Again, we attribute this behaviour to the inclusion of tensor terms for the ρ meson in the effective Lagrangian which induce a different isospin dependent spin-orbit strength compared to the other relativistic models.

The different sequences of nuclei for the parameter sets

of BRUSLIB are nearly on top of each other and are strikingly along the magic neutron numbers 50 and 82. There a only slight differences, as the sequence for set BSk8 reaches $Z = 46$ at $N = 82$, while all other sets from BRUSLIB start the sequence along $N = 82$ at $Z = 44$. The set SLy4 features similar strong correlations in the sequence of nuclei along $N = 50, 82$, but like the relativistic sets NL3 and TMA populates at maximum $Z = 42$ for $N = 82$.

By comparing the sets from BRUSLIB and SLy4 to those of SkM* and SkP one recognizes that the sequences of nuclei from SkM* and SkP are distinctly different in their paths in the nuclear chart as they mainly follow along isotopes and not along the magic neutron numbers 50 and 82. This finding is in stark contrast to the other parameterizations and mass tables used here, making the sets SkP and SkM* noticeable exceptions from our general results.

In particular, the more modern Skyrme HFB mass tables of the sets SLy4 and BSk8 do not exhibit a pronounced sequence along isotopes but are morestuck to the magic neutron numbers 50 and 82. The general trend of the sequence of nuclei being along these magic neutron numbers is supported by the calculation for the FRDM which is strikingly similar to the results for the sets TMA and SLy4. Surprisingly, the classic sequence of BPS, although using rather old mass tables, arrived at a similar sequence for large mass numbers compared to the most modern mass tables!

F. Neutron Driplines and Sequences of Nuclei of State-of-the-Art Nuclear Models

In Fig. 9, we compare the most modern and state-of-the-art mass tables of all the sets listed in Table I. There are no drastic differences in the shape of the neutron dripline. The neutron driplines of all the sets presented in the figure have an approximately linear behaviour extending from $(Z, N) \simeq (20, 46)$ to $(Z, N) = (36, 82)$. At the magic neutron number 82, the neutron driplines suddenly change their slope and follow a vertical path from $(Z, N) = (36, 82)$ to $(Z, N) = (40, 82)$. Note that at the magic neutron number 82, the neutron driplines of all the selected sets are equal. Therefore, the region at $N = 82$ and around $Z = 38$ shows to be the one with the smallest difference in the precise location of the neutron dripline for all modern sets used here. From $(Z, N) = (40, 82)$ to $(Z, N) \simeq (50, 108)$, the neutron driplines again have approximately the same gradient as for low mass numbers. But there are differences in the regions of the nuclide chart where $Z \simeq 28$ and $N \simeq 62$: If one compares the neutron driplines from the mass tables of sets TMA and NL3 (which includes effects from deformations), then one can see that their neutron driplines differ by $\Delta Z = 4$ and $\Delta N = 16$. There are also differences of similar range for the neutron driplines at $(Z, N) \simeq (44, 100)$ if one compares the model TMA with SLy4 and NL3. Also, the sequences of nuclei in β-equilibrium of the modern sets shown do not exhibit pronounced differences, on the contrary, the sequences are nearly on top of each other. There are only small exceptions, as there is a shift to larger proton numbers in the sequence of nuclei for the set BSk8 with $\Delta Z_{\max} = 4$. The sets BSk8 and NL3 have one nucleus in their sequence with $N = 52$, set NL3 ends its sequence at $N = 84$. Besides that and the starting iron and nickel isotopes, the sequences of nuclei for all the selected models and mass tables follow tenaciously the magic neutron numbers 50 and 82 throughout the (unknown) nuclear chart until hitting the neutron dripline.

The endpoint of the sequence of nuclei for all the modern mass tables studied here is quite similar and happens to be at $Z = 34 - 38$ with $N = 82$ ($N = 84$ for the set NL3). In this region of the nuclear chart, the neutron driplines of the various sets examined here do also demonstrate to be rather similar. These features most likely originate from the fact that the magic neutron number 82 prevails up to the neutron dripline in the nuclear mass tables used here, which however, relies on a substantial extrapolation from the masses of known nuclei up to the neutron dripline. Shell quenching effects, as advocated by HZD [17], can possibly exist, in particular for different isospin dependences of the spin-orbit terms. Then the sequence of nuclei as well as its endpoint can be located quite differently as seen e.g. for sets SkM*, SkP and Chiral.

Finally, we note that in all our calculations, there do not appear any super-heavy nuclei in the sequences of nuclei of the nuclear models and sets which we use in this work. We checked that superheavy elements can indeed appear in the sequence of neutron-rich nuclei in the outer crust of neutron stars if we artificially increase their binding energies per nucleon b by about one MeV.

In Fig. 10, we show the dependence of the proton number Z on the mass density ρ by using the representative models of Table I. In this plot, we restrict ourselves to the high mass density region $\rho \geq 10^{10}$ g/cm^3 because for 10^4 g/cm$^3 \lesssim \rho \lesssim 3.5 \times 10^{10}$ g/cm^3 we obtain the same elements for each set as they are fixed by the experimental nuclear data of [25]: $_{26}$Fe, $_{28}$Ni, $_{36}$Kr, $_{34}$Se, $_{32}$Ge, and $_{30}$Zn. For larger mass densities, the proton numbers of most of the sets shown are the same: $_{28}$Ni, $_{42}$Mo, $_{40}$Zr, $_{38}$Sr, and $_{36}$Kr. The only differences for these mass tables is that they arrive at the corresponding proton numbers at different mass densities. For the set TMA, $_{34}$Se and not $_{36}$Kr appears at the highest mass densities in the outer crust of non-accreting cold neutron stars. The set BSk8 is the only one that shows significant differences in comparison to the other sets plotted: For mass densities of $\rho \simeq 10^{11}$ g/cm^3, the BSk8 model has quite different proton numbers as $_{46}$Pd and $_{44}$Ru appear in the sequence of nuclei.

G. Comparison to previous works

In order to compare the sequences of nuclei of BPS [4], HZD [17], and HP [20] with our new results as presented here, we list all the sequences of nuclei of these previous works in tabular form. Table II shows the sequence of nuclei of BPS, Tables III and IV the sequences of nuclei of HZD [17], Tables V and VI the sequences of nuclei of HP [20]. Finally, Tables VII and VIII summarize the sequences of nuclei obtained in this work by using the modern nuclear mass tables from BSk8 and TMA as the characteristic ones of our whole set of mass tables investigated. Note that BPS and HZD only use theoretically computed mass tables, while we, as HP, incorporate experimental data tables in addition. As we know from Fig. 1, the equation of state is not affected significantly by a different sequence of nuclei. That is why we do not show the number density, the pressure and the mass density in every table. Besides that, we are mainly interested in the sequence of nuclei here. As one can see from the tables, the nucleus ^{66}Ni is not present in the crust of non-accreting cold neutron stars if one uses the droplet model from Myers and Swiatecki [16] or the spherical model SkM* from Dobaczewski, Flocard, and Treiner [18]. By taking newer experimental data, this nucleus always exists in the crust. Even with the droplet model of Myers [19], this nucleus is found. A second difference in the sequence of nuclei of BPS [4] compared to HZD, HP, BSk8, and TMA is that in the latter three one, ^{76}Fe never occurs. It only occurs by using the droplet model from Myers and Swiatecki [16] or that one from Myers [19]. When we compare the sequence of nuclei of the model BSk8 with the sequence of nuclei from HZD, HP and that from BPS, we recognize that the nucleus ^{78}Ni is not present in the sequence of nuclei of the model BSk8. The reason why ^{78}Ni appears in the sequence of nuclei from HZD and not in the sequence of nuclei of the BSk8 model is that HZD used the atomic mass table from 1993 [21] and we use the newer one from 2003 [25]. With the set TMA, one obtains a similar sequence of nuclei as for the droplet model of Möller and Nix [22], see Tables V and VIII. The only differences are that by using the set TMA, ^{126}Ru is not present in the sequence of nuclei and that the sequence ends with the nucleus ^{116}Se and not with ^{118}Kr.

The sequence of nuclei obtained by HZD [17] using the set SkP within a spherical calculation of Dobaczewski, Flocard, and Treiner [18] (see table III) is drastically different from all other sequences of nuclei listed here. Unusual nuclei for the crust, such as ^{68}Ni or later in the sequence, nickel nuclei with large neutron numbers appear. In addition, our results for the same set SkP differ from the results of HZD [17]. Note, that the mass table used by HZD is based on a spherical HFB calculation (and a different pairing force) while the one used in this work includes effects from deformations and a modern δ-force pairing. The sequences of nuclei for both mass tables follow closely a certain proton number for a wide range of isotopes, but HZD find $Z = 28$ while we find $Z = 30$ to be prominent. Only the set SkM* shows a similarly wide sequence of nuclei with constant Z, however appearing for $Z = 28$ and not for $Z = 30$. The sequences of nuclei found here differ from the one by HZD also at large mass numbers. HZD find, that the sequence jumps from $Z = 28$ to $Z = 40$ ending with the nucleus ^{134}Zr while the sequence in our calculation populates $Z = 38$ (and once $Z = 26$) and ends with the nucleus ^{126}Sr. We stress, that we compare here different mass tables which are, although based on the same parameter set SkP, computed in significantly different approximations (spherical versus deformed) and use different pairing forces. The general trend of the sequence of neutron-rich nuclei, however, is rather similar, as the sequence follows mainly isotope sequences (constant Z) and not the magic neutron numbers 50 and 82.

The last nucleus in the sequences of nuclei found by using different theoretical nuclear models are shown in Table IX. All of the models listed in Table IX except NL3 and that of [18] have the magic neutron number 82. The charge of the final nucleus of the sequence varies between $Z = 32 - 40$ for previous works while we find a range of $Z = 34 - 38$ for the modern mass tables.

V. SUMMARY AND CONCLUSIONS

In this work, we investigated the outer crust of non-accreting cold neutron stars by using the BPS model and the newest nuclear data. If data from the atomic mass table of 2003 from Audi, Wapstra, and Thibault [25] was available for the corresponding nuclei, we always preferred using this experimental data. We updated previous work of BPS [4], HZD [17], and HP [20] which were based on older data and/or mass parameterizations. We also compared various nuclear models as listed in Table I in order to check their differences concerning the neutron dripline, magic neutron numbers, the equation of state, and the sequence of nuclei in the outer crust of non-accreting cold neutron stars. To our knowledge, this is the first detailed investigation of this kind for an enlarged set of most modern nuclear models and state-of-the-art theoretical mass tables, which entails pairing effects, includes effects of deformation and studies relativistic models in comparison to non-relativistic ones.

We obtain the following results: The equation of state is not affected by small differences in the sequence of nuclei. There are jumps in the mass density at constant pressure if the equilibrium nucleus of the ground state changes to another one. The adiabatic index Γ is not affected by changes in the sequence of nuclei and by using data from different nuclear models. The location of the neutron driplines of the Skyrme type models SkP and SkM* are at smaller proton numbers Z compared to the other Skyrme type models used here (SLy4 and the ones of BRUSLIB). The neutron dripline rises steeper and is nearly linear in mass tables including effects from

deformation as compared to spherical calculations. Pairing has the effect of smoothing out steps on the neutron dripline found when pairing effects are switched off. Besides that, pairing has an impact on the magic neutron numbers towards the neutron driplines. It splits the magic neutron number of the point coupling model PCF1 from 82 to 80 and 82 and the magic neutron number of the chiral model from 70 to 68 and 70. The sequences of nuclei obtained by using theoretical nuclear models can have some differences at large mass numbers A because they predict different binding energies. For low mass numbers, as we use the experimental data from the atomic mass table, the sequences of nuclei in the outer crust of neutron stars are found to be identical. The nucleus ^{66}Ni does not occur in the sequences of nuclei of BPS and HZD but it is present in the sequences of nuclei if one uses newer nuclear data. The sequence of nuclei usually found in all parameterizations used proceeds along the magic neutron numbers 50 and 82 all the way to the neutron dripline. Only the sets for SkP and SkM* show sequences of nuclei which follow a certain (magic) proton number, i.e. $Z = 28, 30$ and $Z = 38$, which is in contrast to all other sets investigated here, being non-relativistic or relativistic ones.

By comparing a selected set of modern models and mass tables, the location of the neutron dripline as well as the sequence of nuclei in β-equilibrium are found to be strikingly similar. The sequence of nuclei follows nearly entirely the magic neutron numbers 50 and 82. The set BSk8 differs slightly from all the other modern models as the sequence of nuclei is shifted to larger proton numbers while following the standard path along $N = 50$ and 82. The endpoint of the sequence coincides with a region in the nuclear chart where the location of the neutron dripline of the various models investigated here coincides. Hence, the final nucleus in the sequence can be pinned down in a rather narrow range and is extracted to be around $Z = 36$ and $N = 82$.

Finally, we note that in all our calculations, there do not appear any super-heavy nuclei in the sequences of nuclei of the nuclear models which we use in this paper. Some of them occur if the binding energies per nucleon b is increased artificially by about one MeV.

The results presented here rely only on the binding energy or mass of neutron-rich isotopes in the range of $Z = 26$ to $Z = 40$, a region of the nuclear chart which will be explored in the near future by the FAIR facility at GSI, Darmstadt, as well as by the ISAC facility at TRIUMF and by the RIA project. With these measurements, the non-relativistic and relativistic models utilized in this work will be tightly constrained on their isospin properties towards the neutron dripline and one can shed more light on the actual sequence of neutron-rich nuclei in the outer crust of neutron stars. We point out that the proton number of nuclei is important for heat transport and for Ohmic dissipation of the magnetic field. Other extraterrestrial sources of information might come from the observations of x-ray binary systems, where a neutron star is accreting material from its stellar companion. X-ray bursts are generated by accretion in the outer crust of neutron stars which transport material of the crust to the surface. The x-ray satellites XMM-Newton, Chandra or in the near future XEUS can give a detailed spectroscopic analysis of an x-ray burst. Cottam, Paerels, and Mendez [49] reported about redshifted spectral lines of highly ionized elements in x-ray bursts of the low-mass x-ray binary EXO 0748-676.

Acknowledgments

We thank Thomas Bürvenich, Thomas Cornelius, Stefan Schramm, and Lisheng Geng for providing the mass tables of the relativistic nuclear models used in this research project. We also thank J. A. Maruhn and P. G. Reinhard for useful discussions. S. R. thanks for using the Center for Scientific Computing (CSC) of the Johann Wolfgang Goethe-Universität. We thank the referee for useful comments. This work is supported by the Gesellschaft für Schwerionenforschung (GSI) in Darmstadt via the program "Fremde F&E-Mittel" in the research project OF/SAF "Struktur von neutronenreichen, exotischen Kernen in der Kruste von Neutronensternen".

[1] R. P. Feynman, N. Metropolis, and E. Teller, Phys. Rev. **75**, 1561 (1949).
[2] E. F. Brown, and L. Bildsten, Ap. J. **496**, 915 (1998).
[3] C. J. Pethick, and D. G. Ravenhall, Annu. Rev. Nucl. Part. Sci. **45**, 429 (1995).
[4] G. Baym, C. Pethick, and P. Sutherland, Ap. J. **170**, 299 (1971).
[5] G. Baym, H. A. Bethe, and C. J. Pethick, Nucl. Phys. **A175**, 225 (1971).
[6] J. W. Negele, and D. Vautherin, Nucl. Phys. **A207**, 298 (1973).
[7] H. Shen, Phys. Rev. C **65**, 035802 (2002).
[8] B. Friedman, and V. R. Pandharipande, Nucl. Phys. **A361**, 502 (1981); A. Akmal, V. R. Pandharipande, and D. G. Ravenhall, Phys. Rev. C **58**, 1804 (1998); M. Baldo, G. F. Burgio, and H. J. Schulze, Phys. Rev. C **61**, 055801 (2000); I. Vidana, A. Polls, A. Ramos, L. Engvik, and M. Hjorth-Jensen, Phys. Rev. C **62**, 035801 (2000).
[9] B. D. Serot, and J. D. Walecka, Advances in Nuclear Physics **16**, ed. J. W. Negele, and E. Vogt (Plenum, NY, 1986); B. D. Serot, Rep. Phys. **55**, 1855 (1992).
[10] N. K. Glendenning, Ap. J. **293**, 470 (1985); P. J. Ellis, R. Knorren, and M. Prakash, Phys. Lett. B **349**, 11 (1995); J. Schaffner, and I. N. Mishustin, Phys. Rev. C **53**, 1416 (1996); R. Knorren, M. Prakash, and P. J. Ellis, Phys. Rev. C **52**, 3470 (1995); H. Huber, F.

Weber, M. K. Weigel, and C. Schaab, Int. J. Mod. Phys. E **7**, 301 (1998); S. Pal, M. Hanauske, I. Zakout, H. Stöcker, and W. Greiner, Phys. Rev. C **60**, 015802 (1999); J. Schaffner-Bielich, M. Hanauske, H. Stöcker, and W. Greiner, Phys. Rev. Lett. **89**, 171101 (2002).

[11] M. Hanauske, D. Zschiesche, S. Pal, S. Schramm, H. Stöcker, W. Greiner, Ap. J. **537**, 958 (2000).

[12] S. Schramm, and D. Zschiesche, J. Phys. G **29**, 531 (2003).

[13] F. Weber, Prog. Part. Nucl. Phys. **54**, 193 (2005).

[14] D. H. Rischke, Prog. Part. Nucl. Phys. **52**, 197 (2004); K. Rajagopal, and F. Wilzcek, hep-ph/0011333; M. Alford, Ann. Rev. Nucl. Part. Sci. **51**, (2001).

[15] S. B. Rüster, I. A. Shovkovy, and D. H. Rischke, Nucl. Phys. **A743**, 127 (2004); K. Fukushima, C. Kouvaris, and K. Rajagopal, Phys. Rev. D **71**, 034002 (2005); I. A. Shovkovy, S. B. Rüster, and D. H. Rischke, J. Phys. G: Nucl. Part. Phys. **31**, S849 (2005); S. B. Rüster, V. Werth, M. Buballa, I. A. Shovkovy, and D. H. Rischke, Phys. Rev. D **72**, 034004 (2005); D. Blaschke, S. Fredriksson, H. Grigorian, A. M. Öztaş, and F. Sandin, hep-ph/0503194; S. B. Rüster, V. Werth, M. Buballa, I. A. Shovkovy, and D. H. Rischke, hep-ph/0509073.

[16] W. D. Myers, and W. J. Swiatecki, UCRL Report 11980 (unpublished); W. D. Myers, and W. J. Swiatecki, Nucl. Phys. **81**, 1 (1966).

[17] P. Haensel, J. L. Zdunik, and J. Dobaczewski, Astron. Astrophys. **222**, 353 (1989).

[18] J. Dobaczewski, H. Flocard, and J. Treiner, Nucl. Phys. **A422**, 103 (1984).

[19] W. D. Myers, *Droplet Model of Atomic Nucleus*, Plenum, New York (1977).

[20] P. Haensel, and B. Pichon, Astron. Astrophys. **283**, 313 (1994).

[21] G. Audi, and A. H. Wapstra, Nucl. Phys. **A565**, 1 (1993).

[22] P. Möller, and J. R. Nix, Atom. Data Nucl. Data Tables **39**, 213 (1988).

[23] Y. Aboussir, J. M. Pearson, A. K. Dutta, and F. Tondeur, Nucl. Phys. **A549**, 155 (1992).

[24] P. Haensel, *Neutron Star Crusts*, *Physics of Neutron Star Interiors*, Lecture Notes in Physics **578**, Springer Verlag Heidelberg, 127 (2001).

[25] G. Audi, A. H. Wapstra, and C. Thibault, Nucl. Phys. **A729**, 337 (2003).

[26] F. Tondeur, S. Goriely, J. M. Pearson, and M. Onsi, Phys. Rev. C **62**, 024308 (2000); S. Goriely, J. M. Pearson, and F. Tondeur, At. Data and Nucl. Data Tables **77**, 311 (2001); Nuclear data downloaded from BRUSLIB: http://www-astro.ulb.ac.be/Html/masses.html.

[27] M. Samyn, S. Goriely, P.-H. Heenen, J. M. Pearson, and F. Tondeur, Nucl. Phys. **A700**, 142 (2001); S. Goriely, M. Samyn, P.-H. Heenen, J. M. Pearson, and F. Tondeur, Phys. Rev. C **66**, 024326 (2002); M. Samyn, S. Goriely, and J. M. Pearson, Nucl. Phys. **A725**, 69 (2003); S. Goriely, M. Samyn, M. Bender, and J. M. Pearson, Phys. Rev. C **68**, 054325 (2003); M. Samyn, S. Goriely, M. Bender, and J. M. Pearson, Phys. Rev. C **70**, 044309 (2004); S. Goriely, M. Samyn, J. M. Pearson, and M. Onsi, Nucl. Phys. **A750**, 425 (2005). Nuclear data downloaded from BRUSLIB: http://www-astro.ulb.ac.be/Html/masses.html.

[28] M. V. Stoitsov, J. Dobaczewski, W. Nazarewicz, S. Pittel, and D. J. Dean, Phys. Rev. C **68**, 054312 (2003); J. Dobaczewski, M. V. Stoitsov, W. Nazarewicz, AIP Conference Proceedings Volume **726**, ed. R. Bijker, R. F. Casten, A. Frank (American Institute of Physics, New York, 2004) p. 51, nucl-th/0404077; Nuclear data downloaded from: http://www.fuw.edu.pl/∼dobaczew/thodri/thodri.html.

[29] L. S. Geng, H. Toki, and J. Meng, Prog. Theor. Phys. **113**, 785 (2005); Lisheng Geng, private communications.

[30] http://www.gsi.de/fair.

[31] http://www.triumf.info.

[32] http://www.orau.org/ria.

[33] R. A. Coldwell-Horsfall, and A. A. Maradudin, J. Math. Phys. **1**, 395 (1960).

[34] P. Möller, J. R. Nix, W. D. Myers, and W. J. Swiatecki, Atom. Data Nucl. Data Tabl. **59**, 185 (1995); P. Möller, J. R. Nix, and K. L. Kratz, Atom. Data Nucl. Data Tabl. **66**, 131 (1997).

[35] J. Bartel, P. Quentin, M. Brack, C. Guet, and H. B. Hakansson, Nucl. Phys. **A386**, 79 (1982).

[36] J. Dobaczewski, H. Flocard, and J. Treiner, Nucl. Phys. **A422**, 103 (1984).

[37] E. Chabanat, P. Bonche, P. Haensel, J. Meyer, and R. Schaeffer, Nucl. Phys. **A627**, 710 (1997); Nucl. Phys. **A635**, 231 (1998), erratum: ibid. **A643**, 441 (1998).

[38] H. Krivine, J. Treiner, O. Bohigas, Nucl. Phys. **A336**, 155 (1980).

[39] R. B. Wiringa, V. Fiks, and A. Fabrocini, Phys. Rev. C **38**, 1010 (1988).

[40] P. Papazoglou, D. Zschiesche, S. Schramm, J. Schaffner-Bielich, H. Stöcker, and W. Greiner, Phys. Rev. C **59**, 411 (1999).

[41] C. Beckmann, P. Papazoglou, D. Zschiesche, S. Schramm, H. Stöcker, and W. Greiner, Phys. Rev. C **65**, 024301 (2002).

[42] S. Schramm, Phys. Rev. C **66**, 064310 (2002).

[43] S. Schramm, Phys. Lett. B **560**, 164 (2003).

[44] G. A. Lalazissis, S. Raman, P. Ring, Atom. Data Nucl. Data Tabl. **71**, 1 (1999).

[45] G. A. Lalazissis, J. König, and P. Ring, Phys. Rev. C **55**, 540 (1997).

[46] M. Bender, K. Rutz, P. G. Reinhard, J. A. Maruhn, and W. Greiner, Phys. Rev. C **60**, 034304 (1999).

[47] T. Bürvenich, D. G. Madland, J. A. Maruhn, P. G. Reinhard, Phys. Rev. C **65**, 044308 (2002).

[48] Y. Sugahara, and H. Toki, Nucl. Phys. A **579**, 557 (1994).

[49] J. Cottam, F. Paerels, and M. Mendez, Nature **420**, 51 (2002).

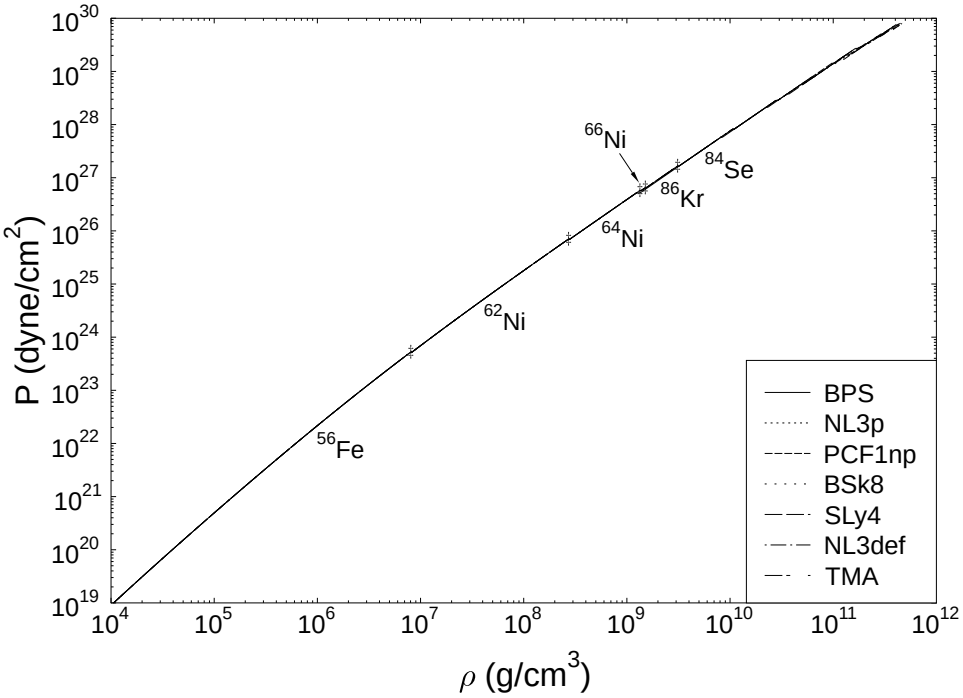

FIG. 1: The equations of state, i.e. the pressures as a function of the mass densities, calculated by using the BPS model and the binding energies of various nuclear models (NL3p: set NL3, spherical calculation with pairing, PCF1np: set PCF1 without pairing, NL3def: set NL3 in the deformed calculation).

μ [MeV]	μ_e [MeV]	$\rho_{\max}$ [g/cm^3]	P [dyne/cm^2]	n_b [cm^{-3}]	Element	Z	N
930.60	0.95	8.09×10^6	5.29×10^{23}	4.88×10^{30}	^{56}Fe	26	30
931.31	2.60	2.69×10^8	6.91×10^{25}	1.62×10^{32}	^{62}Ni	28	34
932.00	4.24	1.24×10^9	5.20×10^{26}	7.48×10^{32}	^{64}Ni	28	36
933.33	7.69	8.15×10^9	5.78×10^{27}	4.90×10^{33}	^{84}Se	34	50
934.42	10.61	2.23×10^{10}	2.12×10^{28}	1.34×10^{34}	^{82}Ge	32	50
935.48	13.58	4.88×10^{10}	5.70×10^{28}	2.93×10^{34}	^{80}Zn	30	50
937.68	19.97	1.63×10^{11}	2.68×10^{29}	9.74×10^{34}	^{78}Ni	28	50
937.78	20.25	1.78×10^{11}	2.84×10^{29}	1.07×10^{35}	^{76}Fe	26	50
937.83	20.50	1.86×10^{11}	2.93×10^{29}	1.12×10^{35}	^{124}Mo	42	82
938.57	22.86	2.67×10^{11}	4.55×10^{29}	1.60×10^{35}	^{122}Zr	40	82
939.29	25.25	3.73×10^{11}	6.79×10^{29}	2.23×10^{35}	^{120}Sr	38	82
939.57	26.19	4.32×10^{11}	7.87×10^{29}	2.59×10^{35}	^{118}Kr	36	82

TABLE II: Sequence of nuclei in the outer crust of non-accreting cold neutron stars calculated by using the nuclear data of Myers and Swiatecki [16] to reproduce the results of BPS [4]. The last line corresponds to the neutron drip point.

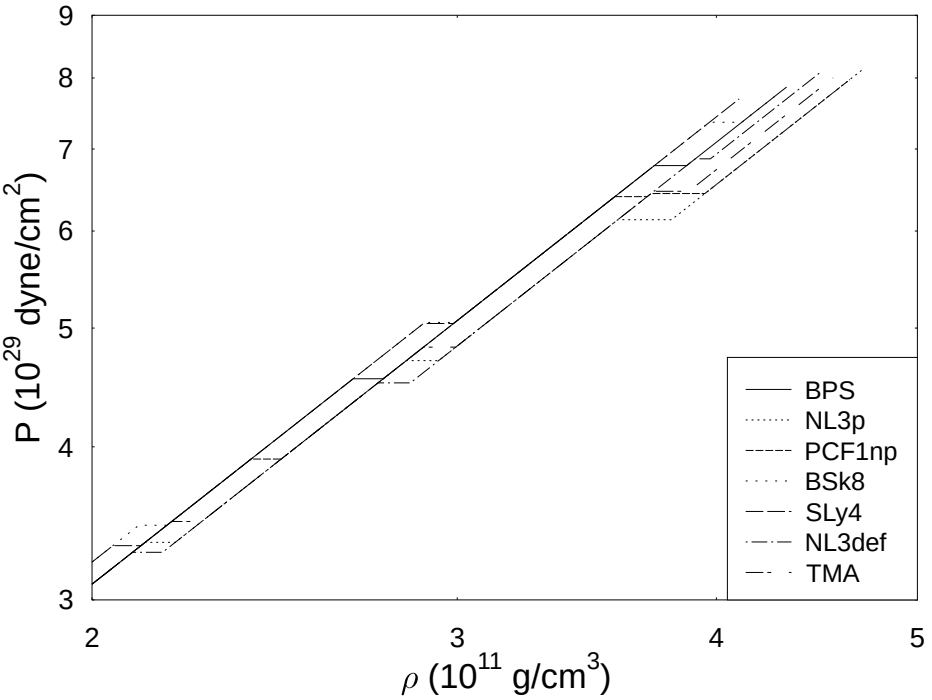

FIG. 2: The same as Fig. 1 for the high mass density range.

μ_e [MeV]	$\rho_{\max}$ [g/cm^3]	Element	Z	N
0.95	7.96×10^6	^{56}Fe	26	56
2.61	2.70×10^8	^{62}Ni	28	34
4.17	1.18×10^9	^{64}Ni	28	36
6.94	5.88×10^9	^{68}Ni	28	40
9.12	1.36×10^{10}	^{84}Se	34	50
9.16	1.40×10^{10}	^{70}Ni	28	42
10.06	1.93×10^{10}	^{72}Ni	28	44
10.86	2.43×10^{10}	^{78}Zn	30	48
13.24	4.52×10^{10}	^{80}Zn	30	50
13.58	4.97×10^{10}	^{76}Ni	28	48
16.51	9.17×10^{10}	^{78}Ni	28	50
18.04	1.23×10^{11}	^{80}Ni	28	52
19.38	1.56×10^{11}	^{82}Ni	28	54
21.12	2.07×10^{11}	^{84}Ni	28	56
22.89	2.70×10^{11}	^{86}Ni	28	58
24.36	3.33×10^{11}	^{88}Ni	28	60
25.10	3.77×10^{11}	^{130}Zr	40	90
25.97	4.25×10^{11}	^{132}Zr	40	92
26.26	4.45×10^{11}	^{134}Zr	40	94

TABLE III: Sequence of nuclei in the outer crust of non-accreting cold neutron stars as calculated by Haensel, Zdunik, and Dobaczewski [17]. Nuclear masses are taken from a spherical calculation using the parameter set SkP of Dobaczewski, Flocard, and Treiner [18].

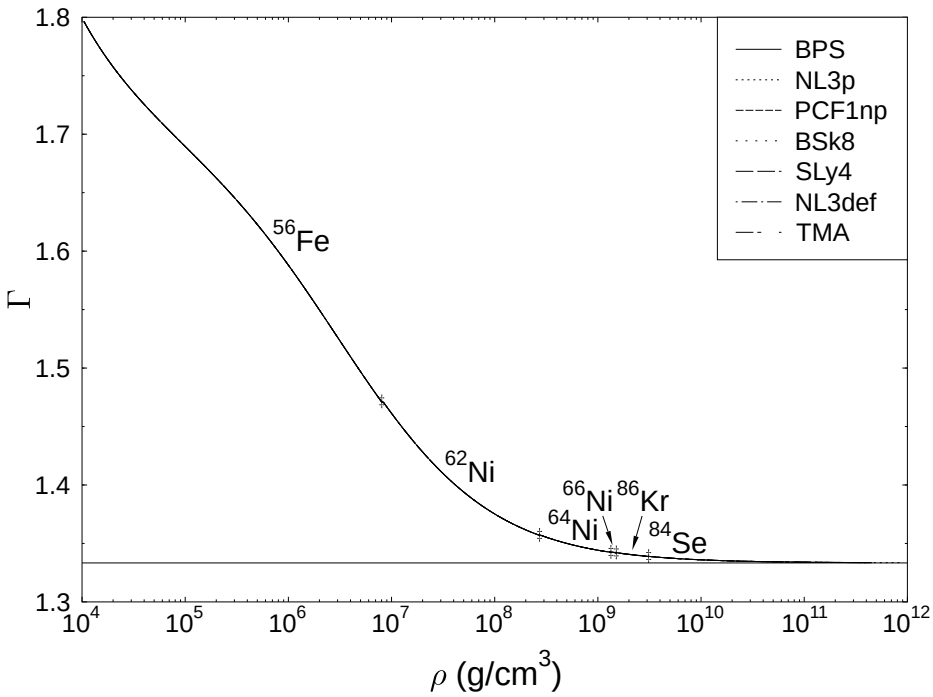

FIG. 3: The adiabatic index as a function of the mass density, calculated by using the BPS model and the binding energies of various nuclear models. The value of Γ of the horizontal line is equal to $\frac{4}{3}$.

μ_e [MeV]	$\rho_{\max}$ [g/cm^3]	Element	Z	N
0.95	7.96×10^6	^{56}Fe	26	30
2.61	2.70×10^8	^{62}Ni	28	34
4.28	1.29×10^9	^{64}Ni	28	36
4.57	1.61×10^9	^{66}Ni	28	38
5.32	2.63×10^9	^{68}Ni	28	40
6.21	4.34×10^9	^{80}Ge	32	48
9.69	1.70×10^{10}	^{82}Ge	32	50
12.26	3.59×10^{10}	^{80}Zn	30	50
18.22	1.23×10^{11}	^{78}Ni	28	50
18.73	1.41×10^{11}	^{76}Fe	26	50
20.15	1.83×10^{11}	^{122}Zr	40	82
22.19	2.53×10^{11}	^{120}Sr	38	82
24.24	3.42×10^{11}	^{118}Kr	36	82
26.28	4.55×10^{11}	^{116}Se	34	82
26.82	5.05×10^{11}	^{114}Ge	32	82

TABLE IV: Sequence of nuclei in the outer crust of non-accreting cold neutron stars calculated by Haensel, Zdunik, and Dobaczewski [17]. Nuclear masses are taken from the droplet model of Myers [19].

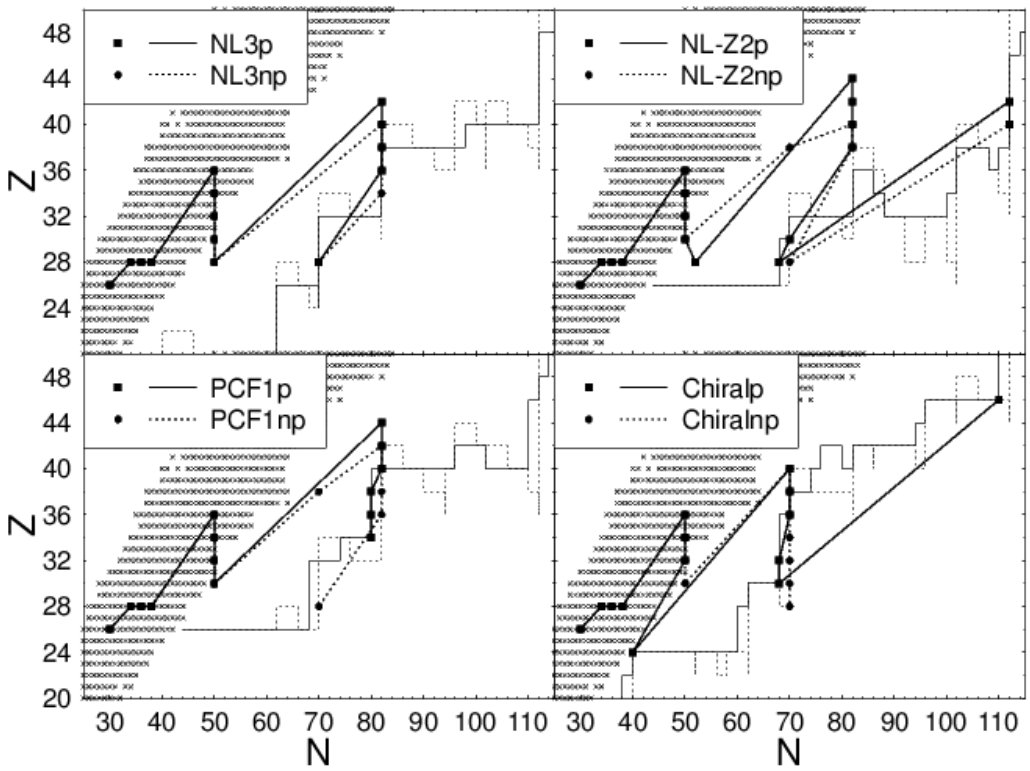

FIG. 4: Nuclear charts of various relativistic nuclear models and their neutron driplines. The upper plots correspond to nuclear models with pairing while the lower ones correspond to nuclear models without pairing. The crosses mark the nuclei which are taken from the atomic mass table [25]. The thick lines and the points show the sequence of nuclei in the outer crust of non-accreting cold neutron stars by using various nuclear data.

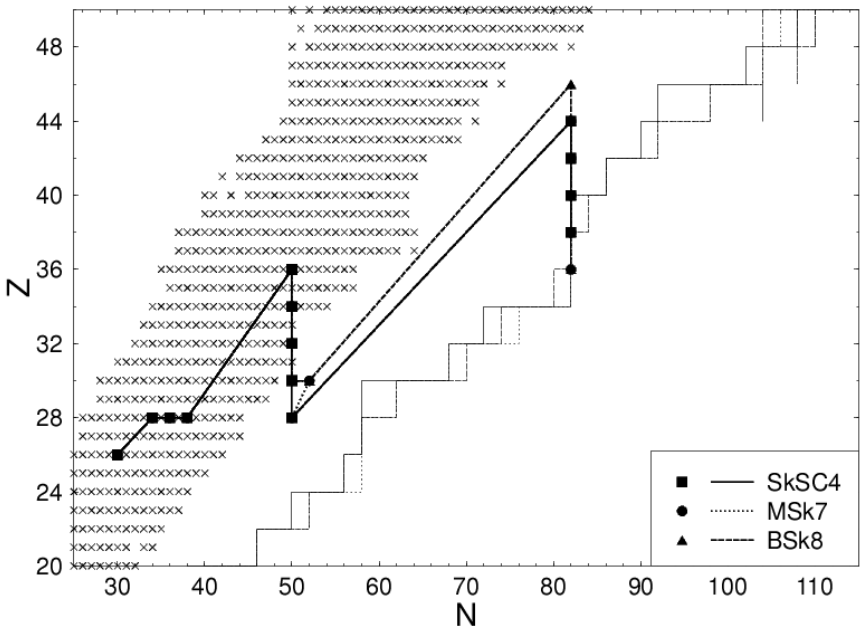

FIG. 5: Nuclear chart of various non-relativistic deformed Skyrme Hartree-Fock-Bogolyubov calculations as taken from BRUSLIB [26, 27] and their neutron driplines. The crosses mark the nuclei which are taken from the atomic mass table [25]. The thick lines and points show the sequence of nuclei in the outer crust of non-accreting cold neutron stars by using various nuclear models.

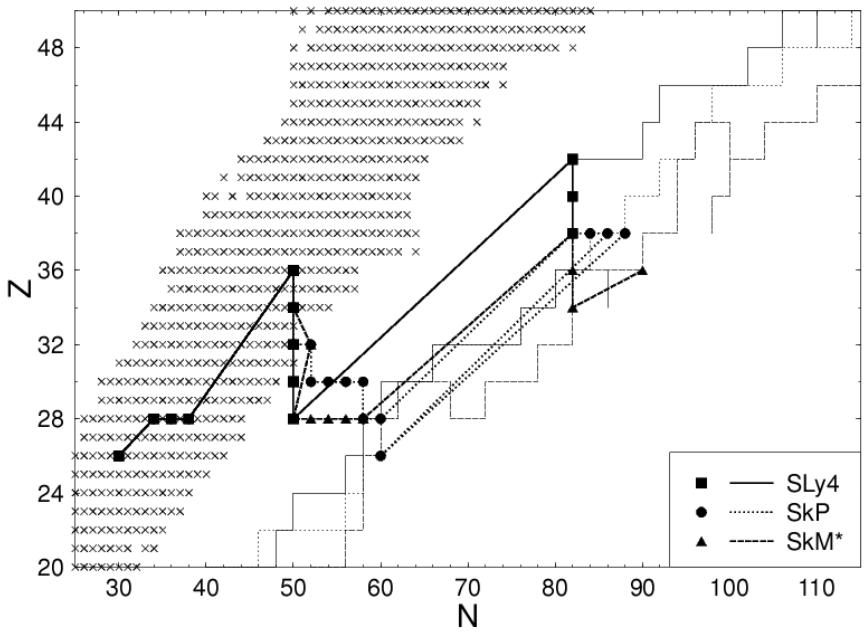

FIG. 6: The same as Fig. 5 but now for non-relativistic deformed Skyrme Hartree-Fock-Bogolyubov models taken from Dobaczewski et al. [28].

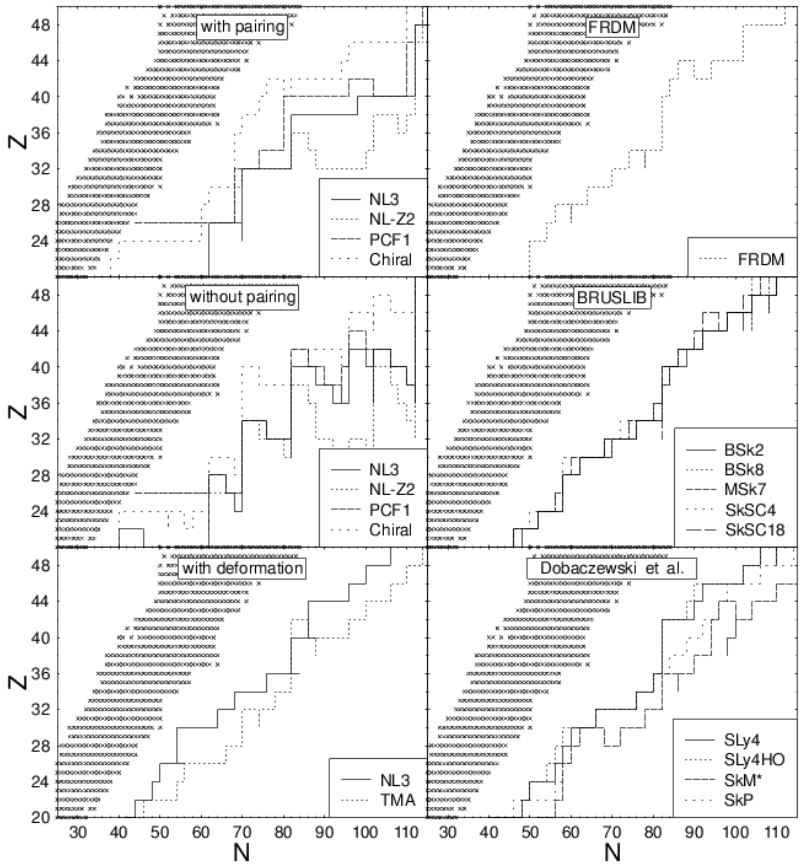

FIG. 7: Nuclear charts showing the neutron driplines of various theoretical nuclear models (see Table I). The crosses mark the nuclei which are taken from the atomic mass table [25].

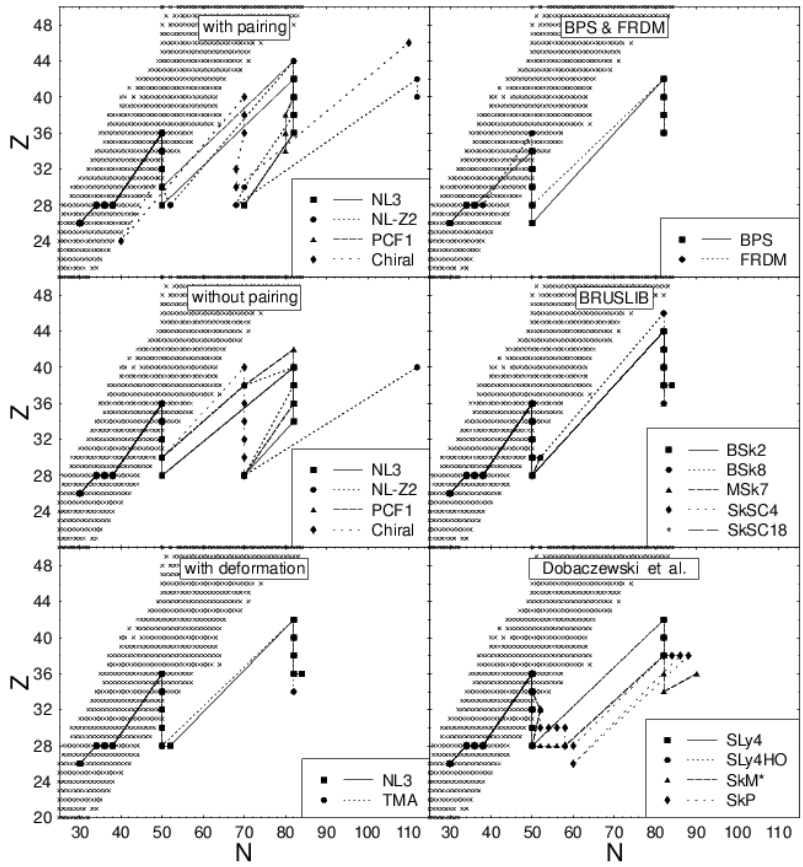

FIG. 8: Same as Fig. 7 but plotting here the sequence of nuclei in the outer crust of non-accreting cold neutron stars by using various nuclear models.

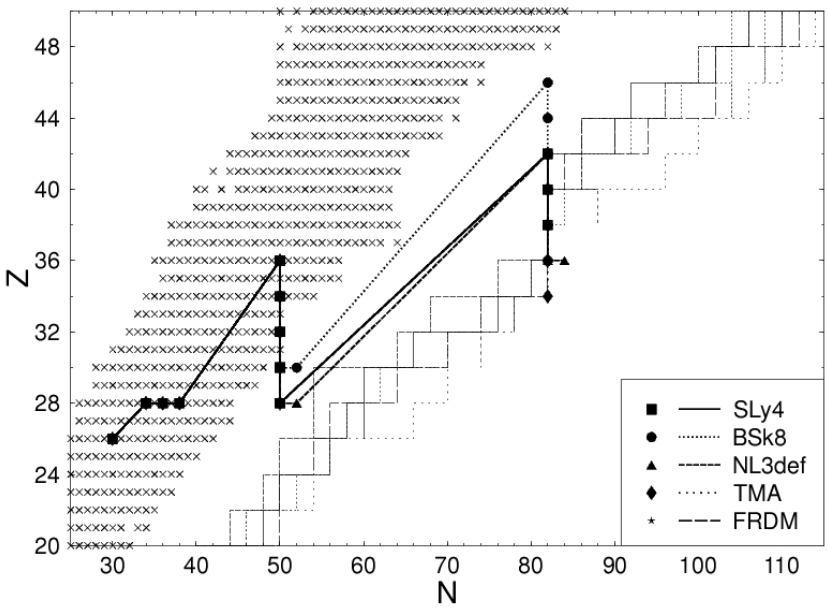

FIG. 9: Nuclear chart of the selected most modern models from Table I and their neutron driplines. The crosses mark the nuclei which are taken from the atomic mass table [25]. The thick lines and points show the sequence of nuclei in the outer crust of non-accreting cold neutron stars.

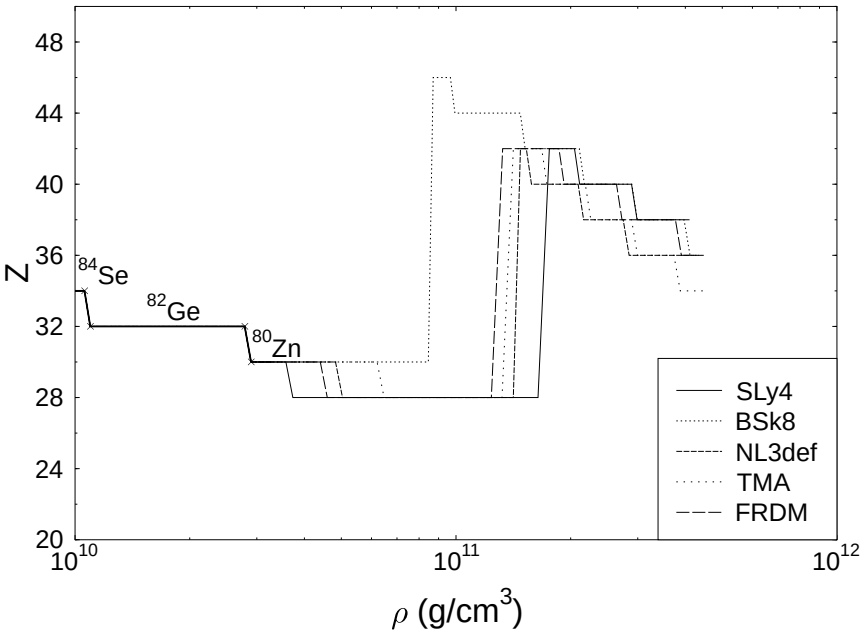

FIG. 10: The proton number Z as a function of the mass density ρ for the selected most modern models as depicted also in Fig. 9.

μ_e [MeV]	$\rho_{\max}$ [g/cm^3]	Element	Z	N
0.95	7.96×10^6	^{56}Fe	26	30
2.61	2.71×10^8	^{62}Ni	28	34
4.31	1.30×10^9	^{64}Ni	28	36
4.45	1.48×10^9	^{66}Ni	28	38
5.66	3.12×10^9	^{86}Kr	36	50
8.49	1.10×10^{10}	^{84}Se	34	50
11.44	2.80×10^{10}	^{82}Ge	32	50
14.08	5.44×10^{10}	^{80}Zn	30	50
16.78	9.64×10^{10}	^{78}Ni	28	50
18.34	1.29×10^{11}	^{126}Ru	44	82
20.56	1.88×10^{11}	^{124}Mo	42	82
22.86	2.67×10^{11}	^{122}Zr	40	82
25.38	3.79×10^{11}	^{120}Sr	38	82
26.19	4.33×10^{11}	^{118}Kr	36	82

TABLE V: Sequence of nuclei in the outer crust of non-accreting cold neutron stars calculated by Haensel and Pichon [20]. Upper part: using experimental nuclear masses. Lower part: using binding energies from the mass formula of Möller and Nix [22]. The last line corresponds to the neutron drip point.

μ_e [MeV]	$\rho_{\max}$ [g/cm^3]	Element	Z	N
17.44	1.08×10^{11}	^{78}Ni	28	50
19.13	1.47×10^{11}	^{126}Ru	44	82
21.66	2.20×10^{11}	^{124}Mo	42	82
24.13	3.15×10^{11}	^{122}Zr	40	82
26.05	4.10×10^{11}	^{120}Sr	38	82

TABLE VI: Sequence of nuclei in the outer crust of non-accreting cold neutron stars calculated by Haensel and Pichon [20]. Upper part: last experimental nuclear mass. Lower part: using the mass formula of Aboussir et al. [23]. The last line corresponds to the neutron drip point.

μ [MeV]	μ_e [MeV]	$\rho_{\max}$ [g/cm^3]	P [dyne/cm^2]	n_b [cm^{-3}]	Element	Z	N
930.60	0.95	8.02×10^{6}	5.22×10^{23}	4.83×10^{30}	^{56}Fe	26	30
931.32	2.61	2.71×10^{8}	6.98×10^{25}	1.63×10^{32}	^{62}Ni	28	34
932.04	4.34	1.33×10^{9}	5.72×10^{26}	8.03×10^{32}	^{64}Ni	28	36
932.09	4.46	1.50×10^{9}	6.44×10^{26}	9.04×10^{32}	^{66}Ni	28	38
932.56	5.64	3.09×10^{9}	1.65×10^{27}	1.86×10^{33}	^{86}Kr	36	50
933.62	8.38	1.06×10^{10}	8.19×10^{27}	6.37×10^{33}	^{84}Se	34	50
934.75	11.43	2.79×10^{10}	2.85×10^{28}	1.68×10^{34}	^{82}Ge	32	50
935.89	14.61	6.07×10^{10}	7.63×10^{28}	3.65×10^{34}	^{80}Zn	30	50
936.44	16.17	8.46×10^{10}	1.15×10^{29}	5.08×10^{34}	^{82}Zn	30	52
936.63	16.81	9.67×10^{10}	1.32×10^{29}	5.80×10^{34}	^{128}Pd	46	82
937.41	19.16	1.47×10^{11}	2.23×10^{29}	8.84×10^{34}	^{126}Ru	44	82
938.12	21.35	2.11×10^{11}	3.45×10^{29}	1.26×10^{35}	^{124}Mo	42	82
938.78	23.47	2.89×10^{11}	5.05×10^{29}	1.73×10^{35}	^{122}Zr	40	82
939.47	25.77	3.97×10^{11}	7.36×10^{29}	2.38×10^{35}	^{120}Sr	38	82
939.57	26.09	4.27×10^{11}	7.74×10^{29}	2.56×10^{35}	^{118}Kr	36	82

TABLE VII: Sequence of nuclei in the outer crust of non-accreting cold neutron stars calculated by using the experimental nuclear data from the atomic mass table [25] (upper part), and the theoretical mass table of the Skyrme model BSk8 as listed by BRUSLIB (lower part). Note that the experimental data from the atomic mass table [25] is always taken first if available. The last line corresponds to the neutron drip point.

μ [MeV]	μ_e [MeV]	$\rho_{\max}$ [g/cm^3]	P [dyne/cm^2]	n_b [cm^{-3}]	Element	Z	N
930.60	0.95	8.02×10^{6}	5.22×10^{23}	4.83×10^{30}	^{56}Fe	26	30
931.32	2.61	2.71×10^{8}	6.98×10^{25}	1.63×10^{32}	^{62}Ni	28	34
932.04	4.34	1.33×10^{9}	5.72×10^{26}	8.03×10^{32}	^{64}Ni	28	36
932.09	4.46	1.50×10^{9}	6.44×10^{26}	9.04×10^{32}	^{66}Ni	28	38
932.56	5.64	3.09×10^{9}	1.65×10^{27}	1.86×10^{33}	^{86}Kr	36	50
933.62	8.38	1.06×10^{10}	8.19×10^{27}	6.37×10^{33}	^{84}Se	34	50
934.75	11.43	2.79×10^{10}	2.85×10^{28}	1.68×10^{34}	^{82}Ge	32	50
935.93	14.71	6.21×10^{10}	7.86×10^{28}	3.73×10^{34}	^{80}Zn	30	50
937.28	18.64	1.32×10^{11}	2.03×10^{29}	7.92×10^{34}	^{78}Ni	28	50
937.63	19.80	1.68×10^{11}	2.55×10^{29}	1.01×10^{35}	^{124}Mo	42	82
938.13	21.38	2.18×10^{11}	3.48×10^{29}	1.31×10^{35}	^{122}Zr	40	82
938.67	23.19	2.89×10^{11}	4.82×10^{29}	1.73×10^{35}	^{120}Sr	38	82
939.18	24.94	3.73×10^{11}	6.47×10^{29}	2.23×10^{35}	^{118}Kr	36	82
939.57	26.29	4.55×10^{11}	8.00×10^{29}	2.72×10^{35}	^{116}Se	34	82

TABLE VIII: The same as Table VII but for the relativistic nuclear model TMA.

Year	Element	Z	N	Model	Refs.
1966	^{118}Kr	36	82	Droplet model of Myers and Swiatecki	[16]
1977	^{114}Ge	32	82	Droplet model of Myers	[19]
1984	^{134}Zr	40	94	Skyrme model SkP (spherical)	[18]
1988	^{118}Kr	36	82	Droplet model of Möller and Nix	[22]
1992	^{120}Sr	38	82	Droplet model of Aboussir et al.	[23]
1995	^{118}Kr	36	82	Finite range droplet model FRDM	[34]
1997/1999	^{120}Kr	36	84	NL3 (with deformations)	[44, 45]
1998/2004	^{120}Sr	38	82	SLy4 (with deformations)	[28, 37]
2004	^{118}Kr	36	82	BSk8 (with deformations)	[27]
2005	^{116}Se	34	82	TMA (with deformations)	[29]

TABLE IX: The endpoint of the sequence of nuclei obtained by using different theoretical nuclear models. Upper part: results obtained in previous work by BPS, HZD, and HP with older nuclear models. Lower part: results obtained in this work by using modern models and mass tables (see Table I).